Nanoscience and Nanometrology
2018; 4(2): 34-40
http://www.sciencepublishinggroup.com/j/nsnm
doi: 10.11648/j.nsnm.20180402.12
ISSN: 2472-3622 (Print); ISSN: 2472-3630 (Online)

Corrosion Behavior of AA5038 Nanostructured Aluminum Alloy Produced by Accumulative Roll-Bonding

Ali Torkan[1], Amin Rabiei Baboukani[2, *], Iman Khakpour[3]

[1]Department of Materials Engineering, Isfahan University of Technology, Isfahan, Iran

[2]Advanced Materials Research Center, Faculty of Materials Engineering, Najafabad Branch, Islamic Azad University, Najafabad, Iran

[3]School of Metallurgy and Materials Engineering, College of Engineering, University of Tehran, Tehran, Iran

Email address:

Amin_rab22@yahoo.com (A. R. Baboukani)

[*]Corresponding author

To cite this article:

Ali Torkan, Amin Rabiei Baboukani, Iman Khakpour. Corrosion Behavior of AA5038 Nanostructured Aluminum Alloy Produced by Accumulative Roll-Bonding. *Nanoscience and Nanometrology*. Vol. 4, No. 2, 2018, pp. 34-40. doi: 10.11648/j.nsnm.20180402.12

Received: July 13, 2018; **Accepted**: September 30, 2018; **Published**: October 27, 2018

Abstract: Accumulative roll bonding is the only severe plastic deformation process for the industrial production of ultrafine grained sheets with desirable mechanical properties. In the present research, corrosion behavior of nanostructured 5083 Aluminum alloy produced by Accumulative Roll Bonding (ARB) was carried out in 3.5% NaCl solution. Potentiodynamic Polarization tests and electrochemical impedance spectrometry were used to evaluate corrosion behavior of samples and immersion test was applied to evaluate intergranular corrosion behavior. The ARB process was successfully performed up to 6 cycles on 5083 aluminum alloy sheet. In early stages of ARB process, main grains were isolated by boundaries resulted from transformation and then layer structure composed of layer boundaries parallel to the rolling direction was created by increasing ARB cycle. By increasing the cycles distance between layer boundaries is decreased and finally by increasing strain more up to four cycles a structure made up of grains with nano grain size was obtained in result of occurrence of In-situ recrystallization. According to the electrochemical corrosion tests, by increasing number of passes in ARB process, the corrosion current density and corrosion rate was increased. Immersion test also revealed that the aluminum alloy annealed in 413°C and ARB samples are not sensitive to intergranular corrosion.

Keywords: Aluminum, Corrosion Behavior, Accumulative Roll-Bonding, Ultrafine Grain Structures

1. Introduction

Series 5xxx aluminum alloys benefit from appropriate corrosion resistance, mechanical properties, formability, welding capacity and high strength to weight ratio. Aluminum alloy 5038 contains 3.5-5% magnesium that presents the highest mechanical properties among all series 5xxx alloys products [1]. This alloy show appropriate corrosion resistance in corrosive environments [2, 3]. In addition to pitting corrosion which is common in aluminum alloys, 5000 series aluminum alloys are susceptible to intergranular corrosion due to grain boundary precipitates such as the β-phase (Al_3Mg_2), especially for those with Mg levels above 3 wt% [4]. The β-phase has been observed at grain boundaries and the interface between the matrix and Al_6Mn dispersoids. The grain boundary precipitates have been observed at triple points and along grain boundaries [5, 6] with reports of both continuous [7] and discontinuous precipitation [8, 9]. Several sever plastic deformation (SPD) processing techniques such as equal channel angular pressing (ECAP) [10], high-pressure torsion (HPT) [11, 12], multi-axial compressions/forging (MAC/F) and accumulative roll-bonding (ARB) [13, 14] were developed in the past two decades to obtain ultrafine grain (UFG) structures in both bulk and sheet materials. The ARB process is a relatively novel method proposed by Saito et al [13] in order to fabricate a submicron/nanograin structure in various kinds of sheet materials. The accumulative roll-bonding process has several advantages over SPD processes such as no need of high load capacity forming facilities and expensive dies, high productivity and no limit on the amount of material to be produced.

In the ARB process, an extremely high plastic strain was imposed on the materials which results in structural

refinement and increasing the strength without changing specimen dimensions apparently. Little is known about the corrosion behavior of UFG Al-alloys fabricated by ARB process. Naeini et al. [15] showed that pitting corrosion resistance of 5052 aluminum alloy prepared by the accumulative roll-bonding process decreases in 3.5% NaCl solution. They identified fine microstructure and increase in defects density as of this decrease. Wei et al. [16] reported that the corrosion resistance of Al-Mn alloy that have become very granulated improves in simulated seawater (3.5% NaCl) due to decrease in size of $MnAl_6$ particles. Therefore, in this research we produced aluminum alloy nanostructured sheets with the ARB process and evaluated their corrosion behavior in 3.5% NaCl solution.

2. Experimental Procedures

2.1. Specimen Preparation by Means of ARB Process

Chemical composition of AA5083 is shown in table 1. 5083 aluminum sheets were annealed in a furnace at 686 K for 2 hours. For the accumulative roll-bonding process at first, the surface is degreasing in acetone and wire brushing with a stainless steel brush. This treatment was performed to remove surface oxide film and achieve a good bonding between the stacked strips during accumulative roll bonding process [17]. Then, we used copper wires to ensure a firm contact between strips and to prevent strips from slipping against each other during rolling. Finally, rolling with 50٪ reduction without any lubricant at room temperature was performed. These steps present one accumulative roll bounding cycle that can be repeated as many times as described. The roll diameter was 127 mm and the roll peripheral speed was about 1 m/min. This procedure was repeated up to sixth cycle. In order to prevent the propagation of edge cracks, which appeared after several cycles, sample edges were trimmed and smoothed down before each following cycle.

Table 1. *Chemical composition of 5083 aluminum alloy in weight percent.*

AL	Mg	Mn	Fe	Si	Cr	Cu	Ti	Ni	Zn
93.81	4.41	0.596	0.288	0.190	0.187	0.561	0.177	<0.020	0.105

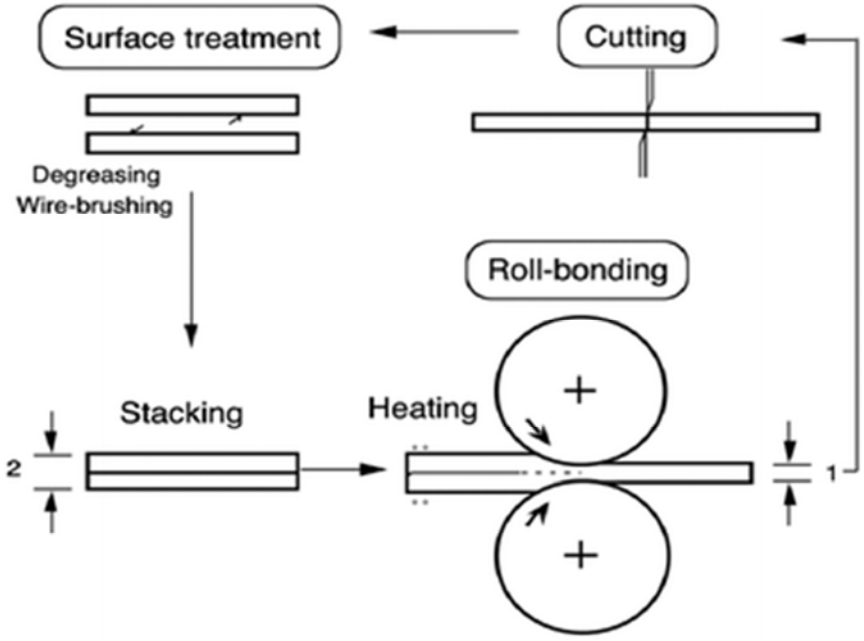

Figure 1. *Schematic illustration of the principle of ARB process.*

2.2. Materials and Microstructure Characterization

The microstructure and selected area diffraction (SAD) patterns of the samples were performed after accumulative roll bonding process by PHILIPS CM200 transmission electron microscopy (TEM) operating at 200 KV. All the microstructures were observed at the rolling direction-normal direction (RD-TD) plane of the strips. TEM samples were mechanically grinded and polished by twin-jet [18]. Specimens' area was observed after performing immersion test using scanning electron microscope (SEM) Philips xl30 model. XRD analyses were performed using X-ray powder diffraction (XRD, Philips X′pert) diffractometer with CoKα radiation (λ = 0.178 nm) generated at 40 kV and 40 mA.

2.3. Electrochemical Assessments and Surface Observations

Corrosion behavior of nanostructured and large grain 5083 aluminum alloys were studied in 3.5% NaCl solution. In the first step, specimens were cut as square in $1\times1cm^2$ dimensions, mounted in resin acrylic, and grinded up to 4000 degree to obtain appropriate surface for corrosion tests. All

open circuit potential (OCP) tests, Potentiodynamic Polarization and electrochemical impedance spectroscopy tests were performed in three-electrode cell. In this cell platinum electrode is used as auxiliary electrode and Ag/AgCl (KCl saturated) is used as reference electrode. AA5083 in 3.5% NaCl solution reaches to open circuit potential after 45minutes. Potentiodynamic Polarization test was performed with Parstat 2273. Potential range is ±250mv than OCP. To investigate corrosion behavior of nanostructured particles further, the electrochemical impedance spectroscopy test was used. These tests were performed in frequency range of 100 KHz-10 mHz with wave amplitude of 10mv. Also to change data obtained by electrochemical impedance spectroscopy, data were modeled using Z-view software and electric circuit was obtained. The immersion test was performed according to the ASTMG67 standard [19]. This test includes immersion of specimens in 30°C (86°F temperature) for 24 hours and determines weight decrease per unit area that is measured as a criterion to determine intergranular corrosion sensitivity.

3. Results and Discussion

3.1. TEM Microstructure

Figure 2 shows TEM images, diffraction pattern and microstructure selected for ARB six-cycle specimen in room temperature. According to the TEM images, very fine grained structure in ARB six-cycle specimen has dominated. In this research size of grains reached to 10 nm after 6 ARB cycles while grains finer than 50 nm and shear nano bonds finer than 10 nm are frequently seen in the structure. SAD pattern of this specimen (figure 2, b) is almost a complete loop indicating presence of many large angle grain boundaries [20].

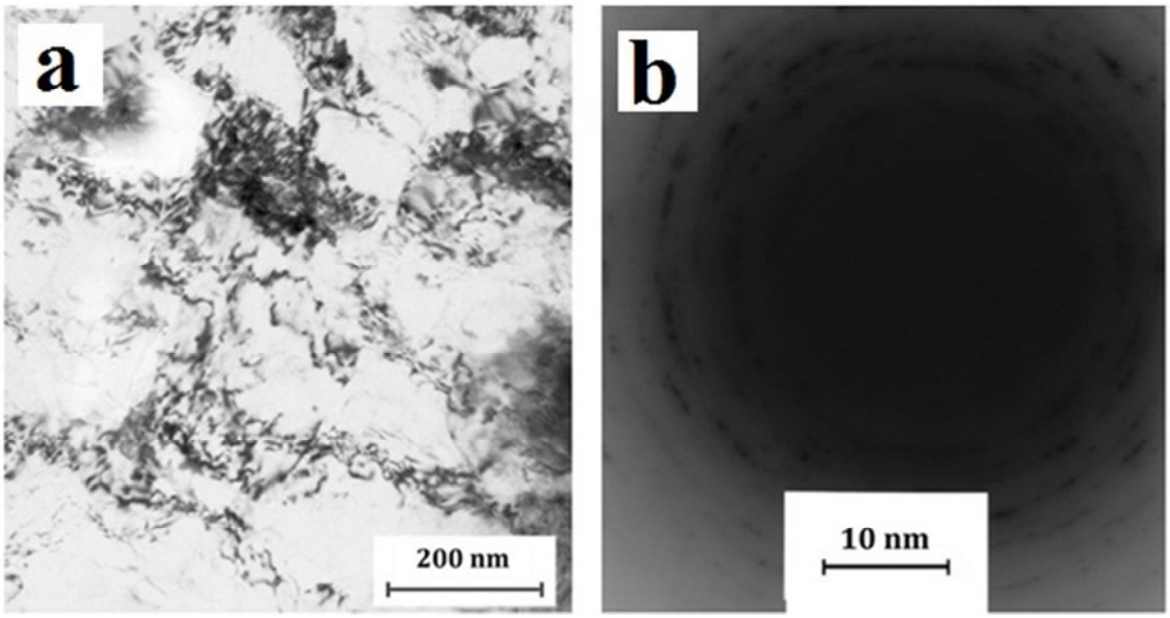

Figure 2. *a) TEM micrographs and b) corresponding SAD pattern of AA 5083 specimen ARBed by 6 passes.*

3.2. Electrochemical Experiments

Potentiodynamic Polarization curves of annealed and ARB specimens in passes of 2, 4 and 6 in 3.5% NaCl solution has been shown in the figure 3. As observed in the figure 3, AA5083 in 3.5% NaCl solution do not show any passivity area that its reason is destruction of passive layer in the 3.5% NaCl solution. Corrosion current density (i_{corr}) and corrosion potential (E_{corr}) of annealed and ARB specimens in different cycles have been presented in the table 2. E_{corr} does not show significant changes while corrosion current density is increased by the number of ARB passes [21]. Therefore, with regard to the fact that i_{corr} is a criterion of corrosion rate, corrosion rate is increased by increasing the number of ARB passes [22].

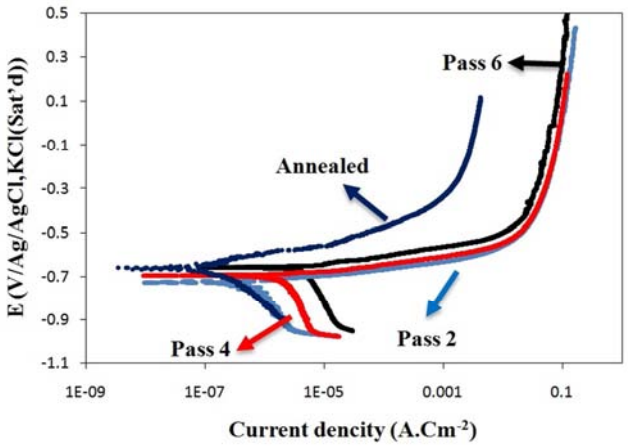

Figure 3. *Potentiodynamic polarization curves of annealed, 2 passes, 4 passes and 6 passes ARB-processed samples in 3.5 wt% NaCl solution.*

Table 2. *Corrosion potential and corrosion current density of the samples in 3.5 wt% NaCl solution.*

Samples	Annealed	2 passes ARBed	4 passes ARBed	6 passes ARBed
Corrosion potential(E;V)	-0.667	-0.725	-0.669	-0.695
Current density of corrosion(I;A/Cm^2)	9.726×10^{-8}	5.354×10^{-7}	2.063×10^{-6}	4.487×10^{-6}

Electrochemical impedance curves of annealed and ARBed samples in 3.5% NaCl solution has been presented in the figure 4. This experiment has been performed to study corrosion behavior of annealed and ARB specimens. Z-view software used to analyze the EIS results and to figure out the equivalent circuit. This circuit has a constant time that is attributed to electrical double layer (figure 4). Amounts of polarization and ohmic resistances and capacitance of electrical double layer have been presented in the table 3. By increasing passes of ARB the polarization resistance is decreased [23]. Since polarization resistance (R_P) and capacitance of electrical double layer are different capacitance is increased when ARB passes are increased so corrosion rate is increased [24, 25].

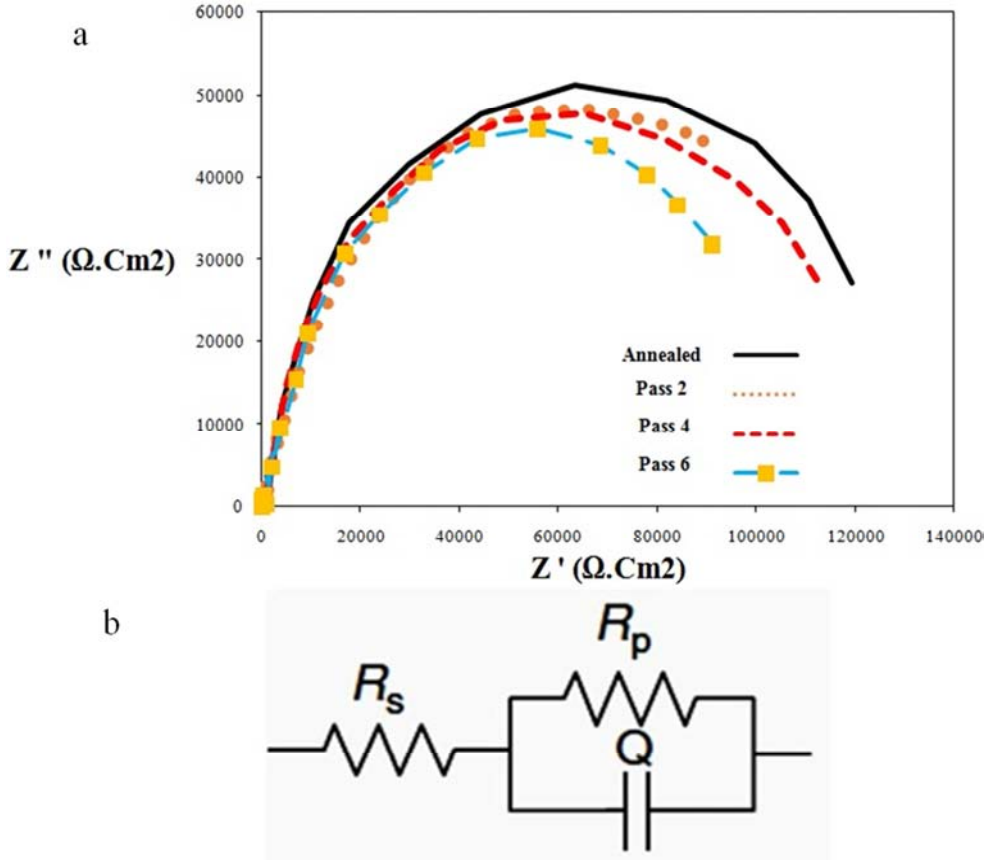

Figure 4. *a) Nyquist plot of impedance spectra of annealed, 2 passes, 4 passes and 6 passes ARB-processed samples in 3.5 wt% NaCl solution and b) equivalent circuit for double layer.*

Table 3. *Amounts of polarization and ohmic resistances and capacitance of electrical double layer of the samples in 3.5 wt% NaCl solution.*

samples	Annealed	2 passes ARBed	4 passes ARBed	6 passes ARBed
Polarization resistance R_p ($\Omega.Cm^2$)	1.2×10^5	1.1×10^5	9.9×10^4	9.6×10^4
capacitance of condenser Q ($\Omega^{-1}.Cm^{-2}.S^{-n}$)	1.60×10^{-6}	1.74×10^{-6}	1.78×10^{-6}	2.06×10^{-6}
Solution resistance R_s ($\Omega.Cm^2$)	9.1	8.9	6.3	7.5

3.3. Immersion Tests

Immersion test has been utilized to determine the sensitivity of annealed and ARB samples to the intergranular corrosion. Figure 5 shows the SEM images of the samples after the test. Amounts of weight loss and corrosion rates for ARB and annealed specimens have been presented in the table 4. According to the results, by increasing ARB passes, pits become finer and are distributed uniformly. Nitric acid selectively solves β secondary phase (Al_3Mg_2) compare to the Mg formed in aluminum matrix solid solution [26, 27]. As a result when this intermetallic compound precipitates in a form of integrated structure across the grain boundaries, their selective corrosion leads to the separation of the grains from the sample [28].

Grain separations in materials in the range of 1-15 mg/Cm^2 are resistant to the intergranular corrosion and values up to

25-27 mg/Cm^2 are susceptible to the intergranular corrosion [29]. As a results, all the samples in this study are not sensitive to the intergranular corrosion because of primarily annealing in 413°C for 2 hours and precipitations of β-phase inside the grains and by increasing the number of ARB passes, precipitations become finer and are distributed across specimen uniformly

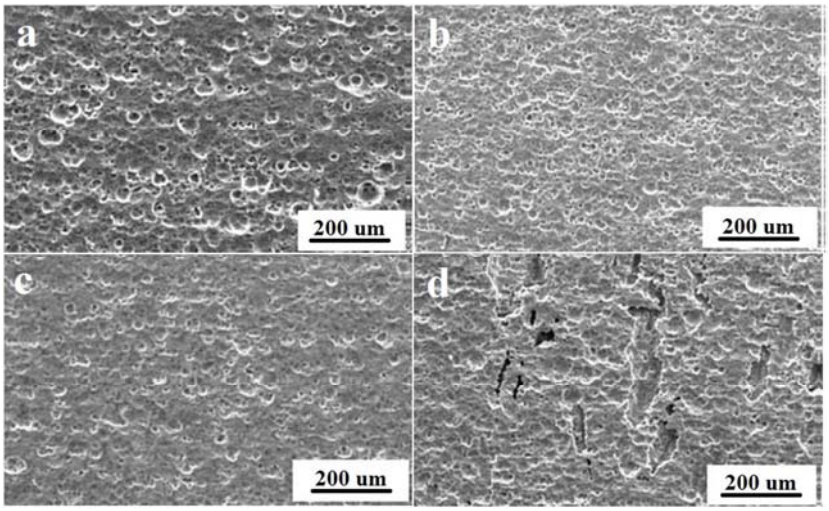

Figure 5. *SEM images immersion samples in Nitric acid solution; a) annealed, b) 2 passes ARBed, c) 4 passes ARBed and d) 6 passes ARBed.*

Table 4. *weight loss and corrosion rate of annealed, 2 passes, 4 passes and 6 passes ARB-processed samples.*

samples	Annealed	2 passes ARBed	4 passes ARBed	6 passes ARBed
Mass loss W; g/cm^2	2.414×10^{-3}	1.922×10^{-3}	1.924×10^{-3}	2.363×10^{-3}
Corrosion rate C.R; mpy	130.456	103.867	103.975	127.700

In order to study the phases in 5083 aluminum alloy annealed in 413°C for 2hours the XRD test was used. Obtained XRD results are presented in the figure 6. As observed, there are three phases of Al_3Mg_2, Mg_2Si and Al_6(Mn, Fe). The intermetallic combination of Al_6(Mn, Fe) is more noble than aluminum matrix and leads to formation of pit in the around matrix. Equation (1) represent the cathodic reaction that occurs in the surface of intermetallic and rich of iron compound [30, 31]. According to the reaction (2), Solubility of aluminum matrix is the main anodic reaction that is performed with cathodic reaction [15].

$$O_2 + 2H_2 + 4e^- \rightarrow 4OH^- \quad (1)$$

$$Al \rightarrow Al^{3+} + 3e^- \quad (2)$$

Intermetallic compound Mg_2Si has relatively similar corrosion potential to it's around matrix and has less corrosion potential than aluminum matrix. Potential of Mg_2Si particles is almost (100-180mv) less than aluminum matrix that indicates anodic behavior of this intermetallic compound [30, 32]. β phase of (Al_3Mg_2) is more active than solid magnesium solution in aluminum and indicates anodic behavior of the β phase than its around matrix [33].

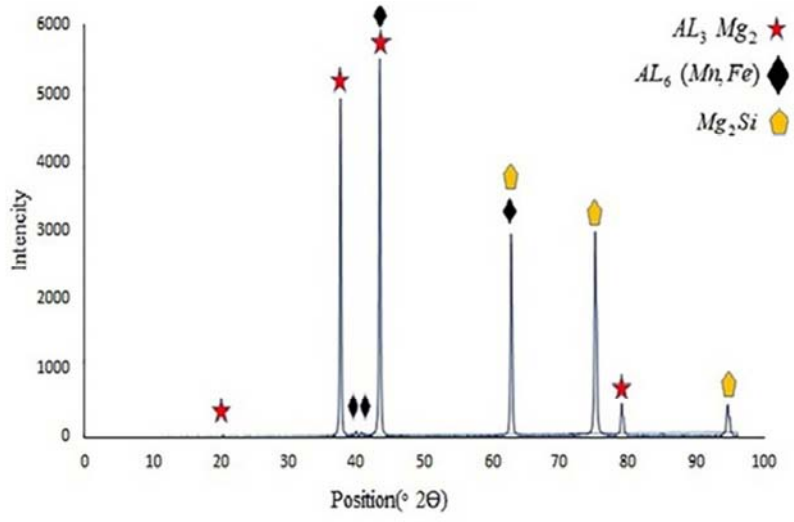

Figure 6. *Diagram of XRD annealed sample in 413°C.*

Forming mechanism of very fine grains during the severe plastic deformation is still discussed. Although recent research have shown that process of forming very fine grains is not process of common and uncontentious recrystallization but has characteristic of In-situ recrystallization [34]. During deformation polycrystalline individual grains can divide into finer grains that are not corresponded. These boundaries are called boundaries resulted from different geometry (GNB). These boundaries separate areas that have transformed by different sliding systems, stress size and different stresses. Also inferior dislocation boundaries (IDB) are available in grains. By increasing stress, nonconformity of GNBs and inferior dislocation boundaries is increased and their distance is decreased. In higher stresses GNBs lead to creating morphology of layer boundaries parallel to rolling direction and connecting boundaries connect layer boundaries to each other [35, 36]. Recrystallization of microstructure by immigration of grain boundary decreased the energy during two main stage. The first stage is breakdown of layer structure. The second stage is spheroidizing. By increasing number of ARB cycles intermetallic phases are broken and change to finer grains. It is expected that by increasing number of passes and after the sixth pass of ARB, size of intermetallic becomes very fine. These intermetallic resist against increase of grain size by preventing growth of grain boundaries like a barrier and prohibit movement of dislocations and With regard to electrochemical characteristics of intermetallic compounds available in 5083 aluminum alloy and by considering microstructure changes provided in this alloy by the ARB process, we observe increase in corrosion rate by increasing number of ARB process passes however, all the samples showing an acceptable intergranular corrosion resistance in corrosive environment [37-39].

4. Conclusion

i. In result of the ARB process such acceptable roll welding is created between layers that in the sixth pass these connections are hard to be distinguished.
ii. Desirable cold welding and grains break down in early stages of the ARB process indicate that the accumulative roll-bonding process is very useful to obtain nanostructure for this alloy. Size of grains reaches to below 100 nm after the sixth cycle.
iii. $Al_6(Fe, Mn)$ particles have more noble potential than the aluminum matrix. Al_3Mg_2, Mg_2Si particles have more active potential than aluminum matrix indicating $Al_6(Fe, Mn)$ particles are cathode than around matrix and Mg_2Si particles are anode than around matrix. Therefore, these particles form galvanic microcells.
iv. In result of the ARB process grain boundaries with small angel change to grain boundaries with large angel and cause finer grains by increases the number of passes. According to the electrochemical corrosion behavior of samples, by increasing the number of passes, galvanic microcells and corrosion rate increased.
v. According to the immersion test, all the samples showed a good resistant against the intergranular corrosion and 6 passes ARB did not make the samples sensitive to intergranular corrosion.

References

[1] Talbot DE, Talbot JD (2018) Corrosion science and technology. CRC press.

[2] Sielski RA (2008) Research needs in aluminum structure. Ships and Offshore Structures 3 (1):57-65.

[3] Mohammadi M, Javadpoura S, Kobayashi A, Shirvani K, Jenabali Jahromi A, Khakpour I (2011) Cyclic oxidation behavior of CoNiCrAlY coatings produced by LVPS and HVOF processes. Transactions of JWRI 40 (1):53-58.

[4] Scamans G, Holroyd N, Tuck C (1987) The role of magnesium segregation in the intergranular stress corrosion cracking of aluminium alloys. Corrosion Science 27 (4):329-347.

[5] Jones RH, Vetrano JS, Windisch Jr C (2004) Stress corrosion cracking of Al-Mg and Mg-Al alloys. Corrosion 60 (12):1144-1154.

[6] Jones R, Baer D, Danielson M, Vetrano J (2001) Role of Mg in the stress corrosion cracking of an Al-Mg alloy. Metallurgical and Materials Transactions A 32 (7):1699-1711.

[7] Yukawa H, Murata Y, Morinaga M, Takahashi Y, Yoshida H (1995) Heterogeneous distributions of Magnesium atoms near the precipitate in Al-Mg based alloys. Acta metallurgica et materialia 43 (2):681-688.

[8] Pickens J, Gordon J, Green J (1983) The effect of loading mode on the stress-corrosion cracking of aluminum alloy 5083. Metallurgical Transactions A 14 (4):925-930.

[9] Khakpour I, Soltani R, Sohi MH (2015) Microstructure and high temperature oxidation behaviour of Zr-doped aluminide coatings fabricated on nickel-based super alloy. Procedia Materials Science 11:515-521.

[10] Valiev RZ, Langdon TG (2006) Principles of equal-channel angular pressing as a processing tool for grain refinement. Progress in materials science 51 (7):881-981.

[11] Valiev RZ, Islamgaliev RK, Alexandrov IV (2000) Bulk nanostructured materials from severe plastic deformation. Progress in materials science 45 (2):103-189.

[12] Foroughi P, Rabiei Baboukani A, Franco Hernandez A, Wang C, Cheng Z (2018) Phase Control during Synthesis of Nanocrystalline Ultrahigh Temperature Tantalum‐Hafnium Diboride Powders. Journal of the American Ceramic Society.

[13] Saito Y, Utsunomiya H, Tsuji N, Sakai T (1999) Novel ultra-high straining process for bulk materials—development of the accumulative roll-bonding (ARB) process. Acta materialia 47 (2):579-583.

[14] Eizadjou M, Manesh HD, Janghorban K (2009) Microstructure and mechanical properties of ultra-fine grains (UFGs) aluminum strips produced by ARB process. Journal of Alloys and Compounds 474 (1-2):406-415.

[15] Naeini MF, Shariat MH, Eizadjou M (2011) On the chloride-induced pitting of ultra fine grains 5052 aluminum alloy produced by accumulative roll bonding process. Journal of Alloys and Compounds 509 (14):4696-4700.

[16] Wei W, Wei KX, Du QB (2007) Corrosion and tensile behaviors of ultra-fine grained Al–Mn alloy produced by accumulative roll bonding. Materials Science and Engineering: A 454:536-541.

[17] Tsuji N, Ito Y, Saito Y, Minamino Y (2002) Strength and ductility of ultrafine grained aluminum and iron produced by ARB and annealing. Scripta Materialia 47 (12):893-899.

[18] Rezayan AH, Firoozi N, Kheirjou S, Rezaei SJT, Nabid MR (2017) Synthesis and Characterization of Biodegradable Semi-Interpenetrating Polymer Networks Based on Star-Shaped Copolymers of ε-Caprolactone and Lactide. Iranian journal of pharmaceutical research: IJPR 16(1):63.

[19] ASTM International WC, PA. (2004) ASTM G67-04, "Standard Test Method for Determining the Susceptibility to Intergranular Corrosion of 5XXX Series Aluminum Alloys by Mass Loss After Exposure to Nitric Acid (NAMLT Test)".

[20] Firoozi N, Rezayan AH, Tabatabaei Rezaei SJ, Mir-Derikvand M, Nabid MR, Nourmohammadi J, Mohammadnejad Arough J (2017) Synthesis of poly (ε-caprolactone)-based polyurethane semi-interpenetrating polymer networks as scaffolds for skin tissue regeneration. International Journal of Polymeric Materials and Polymeric Biomaterials 66(16):805-811.

[21] Zolfaghari S, Baboukani AR, Ashrafi A, Saatchi A (2018) Investigation the effects of Na2MoO4 as an inhibitor on electrochemical corrosion behavior of 316L stainless steel in LiBr solution. Zaštita materijala 59 (1):108-116.

[22] Baboukani AR, Sharifi E, Akhavan S, Saatchi A (2016) Co complexes as a corrosion inhibitor for 316 l stainless steel in H2SO4 solution. Journal of Materials Science and Chemical Engineering 4 (09):28.

[23] Hassannejad H, Moghaddasi M, Saebnoori E, Baboukani AR (2017) Microstructure, deposition mechanism and corrosion behavior of nanostructured cerium oxide conversion coating modified with chitosan on AA2024 aluminum alloy. Journal of Alloys and Compounds 725:968-975.

[24] Baboukani AR, Saatchi A, Wang C Electrochemical Corrosion Behavior of Ti-6Al-4V Alloy Using Akermanite As a Bioceramic Coating. In: Meeting Abstracts, 2018. vol 14. The Electrochemical Society, pp 1043-1043.

[25] Saberi F, Boroujeny BS, Doostmohamdi A, Baboukani AR, Asadikiya M (2018) Electrophoretic deposition kinetics and properties of ZrO2 nano coatings. Materials Chemistry and Physics 213:444-454.

[26] Sharma MM, Ziemian CW (2008) Pitting and stress corrosion cracking susceptibility of nanostructured Al-Mg alloys in natural and artificial environments. Journal of materials engineering and performance 17 (6):870-878.

[27] Khoshkhou Z, Torkghashghaei M, Baboukani AR (2018) Corrosion Inhibition of Henna Extract on Carbon Steel with Hybrid Coating TMSM-PMMA in HCL Solution. Open Journal of Synthesis Theory and Applications 7 (01):1.

[28] Fadavi M, Baboukani AR, Edris H, Salehi M (2018) Study on High-Temperature Oxidation Behaviors of Plasma-Sprayed TiB2-Co Composite Coatings. Journal of the Korean Ceramic Society 55 (2):178-184.

[29] Schacht M, Boukis N, Dinjus E (2000) Corrosion of alumina ceramics in acidic aqueous solutions at high temperatures and pressures. Journal of materials science 35 (24):6251-6258.

[30] Yasakau K, Zheludkevich M, Ferreira M (2017) Role of intermetallics in corrosion of aluminum alloys. Smart corrosion protection. In: Intermetallic Matrix Composites. Elsevier, pp 425-462.

[31] Baboukani AR, Adelowo E, Agrawal R, Khakpour I, Drozd V, Li W, Wang C (2018) Electrostatic Spray Deposited Sn-SnO2-CNF Composite Anodes for Lithium Ion Storage. ECS Transactions 85 (13):331-336.

[32] Tsuji N, Saito Y, Lee SH, Minamino Y (2003) ARB (Accumulative Roll‐Bonding) and other new techniques to produce bulk ultrafine grained materials. Advanced Engineering Materials 5 (5):338-344.

[33] Holtz RL, Goswami R, Pao PS (2015) Sensitization of Naturally Aged Aluminum 5083 Armor Plate. NAVAL RESEARCH LAB WASHINGTON DC MATERIALS SCIENCE AND TECHNOLOGY DIV.

[34] Gashti S, Fattah-Alhosseini A, Mazaheri Y, Keshavarz M (2016) Effects of grain size and dislocation density on strain hardening behavior of ultrafine grained AA1050 processed by accumulative roll bonding. Journal of Alloys and Compounds 658:854-861.

[35] Kassner M, Barrabes S (2005) New developments in geometric dynamic recrystallization. Materials Science and Engineering: A 410:152-155.

[36] Li BL, Tsuji N, Minamino Y Microstructural evolution in 36% Ni austenitic steel during the ARB process. In: Materials science forum, 2006. Trans Tech Publ, pp 73-78.

[37] Gholinia A, Humphreys F, Prangnell P (2002) Production of ultra-fine grain microstructures in Al–Mg alloys by coventional rolling. Acta materialia 50 (18):4461-4476.

[38] Rollett A, Humphreys F, Rohrer GS, Hatherly M (2004) Recrystallization and related annealing phenomena. Elsevier.

[39] Moschouris K, Firoozi N, Kang Y, (2016) The application of cell sheet engineering in the vascularization of tissue regeneration. 11 (6): 559-570.